

Undercooling and Microstructure of Gas Atomized Ni-based Superalloy Powders

Chen Shiqi¹, Lu Zhi², Wang Guangxin²

¹ State Key Laboratory of Powder Metallurgy, Central South University, Changsha 410083, China; ² Research Center for High Purity Materials, Henan University of Science and Technology, Luoyang 471023, China

Abstract: Atomization is an effective approach to obtain fine and spherical alloy powders. Undercooling is an important factor that can affect the property of powders during atomization. The effects of powder size and cooling rate on the undercooling and microstructure of powders were investigated, and the relation between powder size, cooling rate and undercooling was obtained through DSC. The results show that a small powder size and a low cooling rate will result in a large undercooling. Meanwhile, it is found that when the undercooling is large, the dendrite arm spacing of the particles decreases. The smaller the powder size, the greater the proportion of cellular grains, and the finer the grain size of the powders.

Key words: atomization; powder; undercooling; Ni-based alloy

Gas atomization is a widely used process for fabricating ultrafine metals and alloy powders^[1,2]. The mechanism is to transfer kinetic energy from the high velocity gas through a nozzle to the liquid flow of metal melt, and then the melt will be crashed and broken up into metal droplets. During falling, the droplets spheroidize, and solidify into solid-state metal powders, whose diameter may range from micrometers to millimeters^[1,3].

Atomization is a technique of rapid solidification processing, which has achieved widespread recognition for the production of improved alloy homogeneity, refined microstructures, novel metastable and amorphous phase^[4-6].

During the atomization process, undercooling is one of the important factors that affect the solidification structure of powders^[7]. Some researchers have investigated the effect of undercooling on the solidification structure of powders, and found that large undercooling is good to the refinement of solidification structure, which can reduce the composition segregation^[7,8]. Mueller et al^[9] have studied the undercooling of aluminum powders by thermal analysis measurements. It is found that the undercooling level may be influenced by a number of variables, including emulsified salt, cooling rate,

melt superheat and particle size, and these variables may influence the nucleation kinetics of the powders. Perepezko et al^[10] have investigated the undercooling and solidification of atomized alloy powders. They found that a high cooling rate could change the level of accessible undercooling. It is easy to form a metastable phase at high undercooling. Furthermore, the kinetic competition near a phase transition may result in drastic microstructure changes that are sensitive to slight variations in processing conditions. Guan et al^[11] have studied the undercooling of droplet solidification of pure aluminum. They found that during solidification, a small droplet size brings a large undercooling. Moreover, high cooling rates will also result in a large undercooling.

In this paper, Ni-based superalloy powders were prepared by close-coupled gas atomization, and spherical and fine powders were obtained. Undercooling and microstructure of gas atomized Ni-based superalloy powders were studied, especially the effect of powder size and cooling rate on the undercooling of powders.

1 Experiment

The nominal composition (wt%) of the Ni-based alloy used

Received date: December 14, 2017

Foundation item: National Natural Science Foundation of China (U1504516); Educational Commission Foundation of Henan province of China (16A430016)

Corresponding author: Lu Zhi, Ph. D., Research Center for High Purity Materials, Henan University of Science and Technology, Luoyang 471023, P. R. China, E-mail: luzhi02013@163.com

Copyright © 2018, Northwest Institute for Nonferrous Metal Research. Published by Elsevier BV. All rights reserved.

in this paper was : 53Ni-19Cr-4.9Nb-2.8Mo-0.3Al-0.3Ti, and the balance Fe. All the raw materials were vacuum induction melted into a master alloy. The master alloy was remelted at 1973 K, and then the melt was gas atomized in Ar at a pressure of 4 MPa. The atomization process was carried out in a PSI HERMIGA gas atomizer. Fig.1 presents a schematic of the experimental setup of the gas atomizer. The alloy melt was prepared in an intermediate frequency induction furnace, and then the melt export to the atomizing nozzle through a melt delivery tube, which was made of high purity corundum. Meanwhile, high pressure Ar was used to impact the melt to flow out from the melt delivery tube, and then the melt was crushed in small droplets and cooled down into alloy powders. The powder was collected in a powder collector under the atomization chamber.

A certain amount of powders were collected, with the main particle size from 20 μm to 100 μm , and then they were classified into 5 grades by an air classifier system. Subsequently, powders of each grade were dropped into a pure Al_2O_3 crucible used in the differential scanning calorimetry (DSC), which was heated and cooled under a nitrogen atmosphere. Continuous heating and cooling DSC experiments were performed in an STA449 F3 DSC calorimeter (NETZSCH) at a rate of 15 K/min. Moreover, in order to study the effect of cooling rate on the undercooling, the powders of each grade were heated at a given heating rate and then cooled at rates of 5, 10 and 15 K/min.

Each DSC experiment was retested three times and then averaged. The phase structures of the powder were determined by D8 advanced X-ray diffractometer (Bruker) with $\text{Cu K}\alpha$, scanning at a voltage of 40 kV and a speed of 6 $^\circ$ /min. The size and morphology of powders were confirmed using the SIGMA HD field emission scanning electron microscopy (ZEISS). In order to study the microstructure, some of the powder was mixed with resin and ground off to a half, and then polished and etched in a solution composed of distilled water (100 mL), HF (8 mL), HNO_3 (20 mL), $\text{CuCl}_2 \cdot 2\text{H}_2\text{O}$ (3 g).

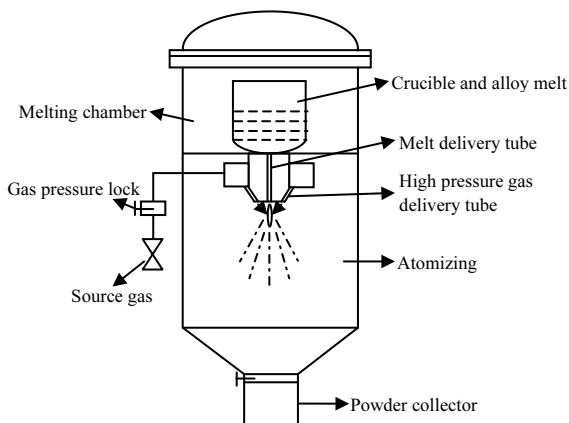


Fig.1 Schematic of experimental setup of the gas atomizer

2 Results

The particle size distribution of Ni-based superalloy powders is shown in Fig.2. The mass fraction of the superfine powders (<38 μm) is about 35%, while that of the coarsest powders (75~150 μm) is about 15% and of other powders (38~48 μm , 48~75 μm) are 26% and 24%, respectively. Therefore, the percent of fine particles is much larger than that of the coarse particles, so gas atomization is an effective method for obtaining fine powder. The formation of fine powder is related to its undercooling and cooling rate^[11,12], so it is important to study these characters of powders. The sizes of powders used in this paper are shown in Table 1. The particle size is divided into five grades, which involve most of the main sizes that we obtain through gas atomization.

The melting and solidification temperature of the powders are obtained by DSC. The DSC results for the powders heated and cooled at a rate of 15 $^\circ\text{C}/\text{min}$ are shown in Fig.3, through which the undercooling of each grade powder can be calculated, as shown in Table 2. As shown in Fig.3, the finer the powder size, the lower the melting and solidification temperatures, and the peak of DSC curves will move more to the lower temperatures. The undercooling of each grade powder is defined as the temperature difference between the melting temperature and the solidification temperature. As shown in Table 2, the finer the powder size, the larger the undercooling. Undercooling is also related to the cooling rate^[9,13], so the undercooling of alloy powder under different cooling rates is selected for further studies. The results of DSC experiment on 20 μm Ni-based superalloy powders at different cooling rates are shown in Fig.4, and the calculated undercooling is listed in Table 3. It is obvious that the undercooling increases with the cooling rate of powders.

The microstructure of powders will be affected significantly by the undercooling. The influence of undercooling on the microstructure of the powders is indicated in Fig.5. For 100 μm

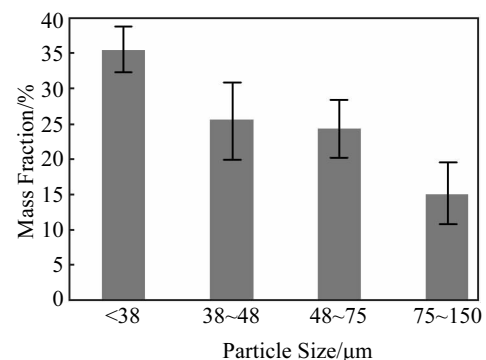


Fig.2 Particle size distribution of Ni-based superalloy powders

Table 1 Average size of the powder of five grades

Powder grade	a	b	c	d	e
Powder size/ μm	100	58	40	25	20

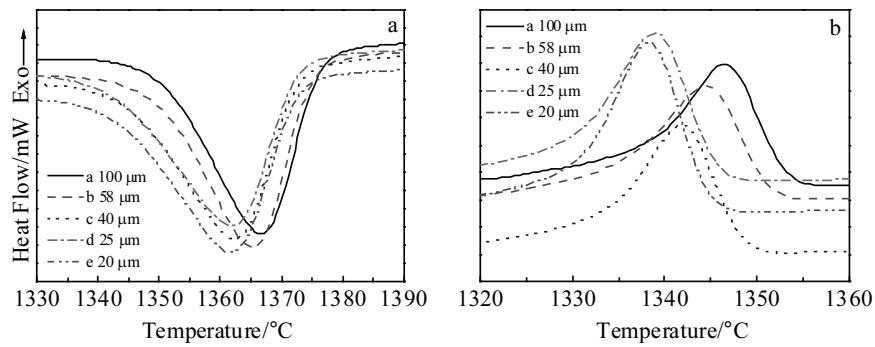


Fig.3 DSC curves of Ni-based superalloy powders with different sizes heated (a) and cooled (b) at the rate of 15 °C/min

Table 2 Powder size and corresponding undercooling calculated by DSC experiments

Powder size, $d/\mu\text{m}$	100	58	40	25	20
Melting temperature, $T_M/^\circ\text{C}$	1366.68	1365.19	1362.26	1361.95	1361.72
Solidification temperature, $T_S/^\circ\text{C}$	1346.51	1344.38	1341.81	1338.94	1338.25
Undercooling, $\Delta T/^\circ\text{C}$	20.17	20.81	20.45	23.01	23.47

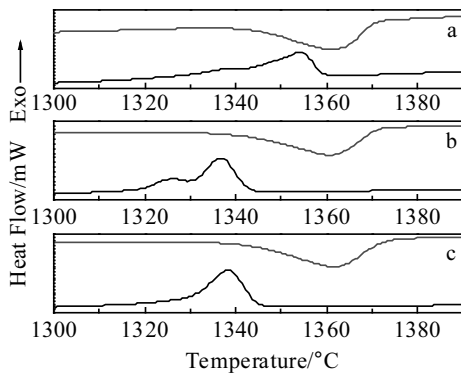


Fig.4 DSC curves of 20 μm Ni-based superalloy powders melted at different cooling rates: (a) 5 °C/min, (b) 10 °C/min, and (c) 15 °C/min

Table 3 Undercooling of 20 μm powder at different cooling rates calculated by DSC

$v/^\circ\text{C}\cdot\text{min}^{-1}$	5	10	15
$T_M/^\circ\text{C}$	1361.26	1360.55	1361.72
$T_S/^\circ\text{C}$	1354.11	1337.61	1338.25
$\Delta T/^\circ\text{C}$	7.15	22.94	23.47

Note: v -cooling rate, T_M -melting temperature, T_S -solidification temperature, ΔT -undercooling, d -powder size

powders, at a low undercooling of 20.17 °C, the microstructure shows a typical solidification feature with dendritic structures, and most of the grain size is more than 5 μm . The surface microstructure of the particles is very clear, and the dendritic boundaries can be detected, as shown in Fig. 5a₁ and 5a₂. As the particle size decreases, the undercooling increases, and the surface of the particles is not as clear as that

of the 100 μm powders. There is no large area of dendritic grains on the surface, but mainly cellular structures, most of which have a grain size of about 2 μm , as shown in Fig.5b₁ and 5b₂. When the particle size is even finer, the undercooling increases to about 23.01 °C, and the surface of the particles is even different from the former, and it is hard to see dendritic boundaries, as shown in Fig.5c₁ and 5c₂. It is believed that particles with a high level of undercooling will have a high cooling rate, which results in a finer microstructure. To further investigate the microstructure of the finer particles, the surfaces were examined by a higher magnification SEM, as can be seen in Fig.6, which is the same particle in Fig.5c. The surface of the particles is full of finer grains with a size of 200 nm, which is the result of high undercooling and cooling rates.

X-ray diffraction analyses indicate that the powders of different sizes have the same phase composition, as is shown in Fig.7, only the alloy phase. No other detectable phases in the powder can be found, so the gas atomization technique is an effective method to obtain pure alloy powders.

3 Discussions

3.1 Effect of particle size on the undercooling of powders

The relation between particle size and undercooling of gas atomized Ni-based superalloy powders is shown in Table 2. It is obvious that the undercooling increases with decreasing particle size, which implies the size effect when the powders solidify from the molten melt droplets whose size is approximately equal to the powder size, and the droplets are close to spherical. Then the effect of powder size on the solidification of melt droplets can be expressed by the following function^[9,11]:

$$X = \exp[-Ma] \quad (1)$$

where X is nucleant-free powder fraction, a is powder

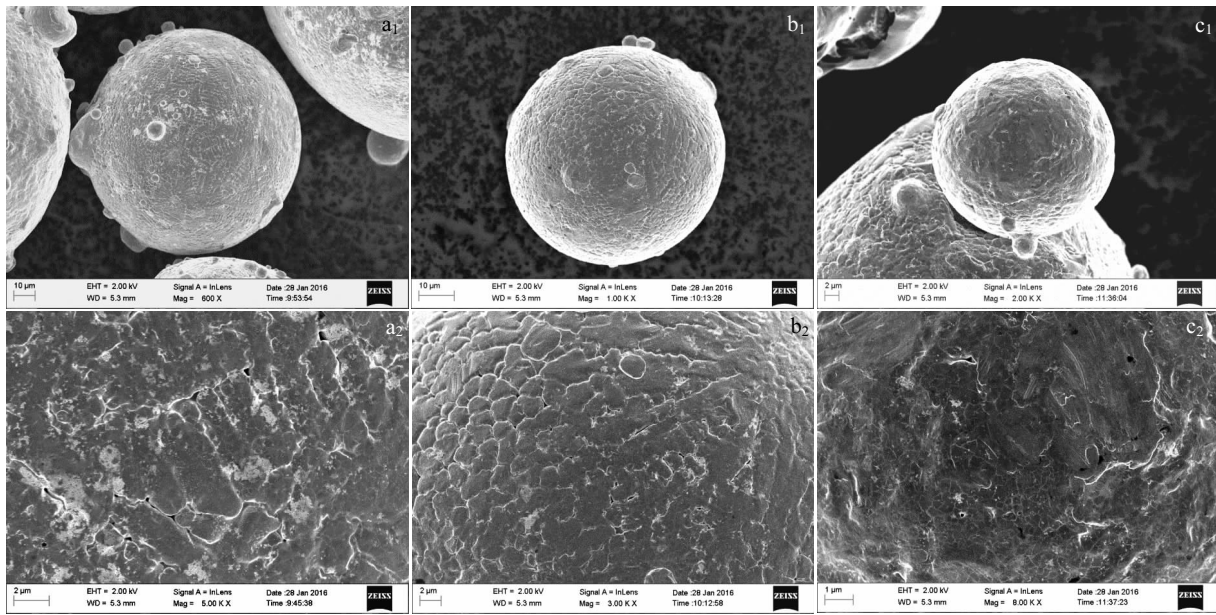


Fig.5 Microstructures of gas atomized Ni-based superalloy powders with different particle sizes: (a₁, a₂) 100 μm, (b₁, b₂) 62 μm, and (c₁, c₂) 26 μm

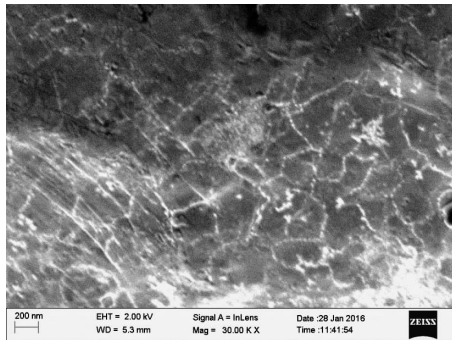


Fig.6 High magnification SEM micrograph of 26 μm powder

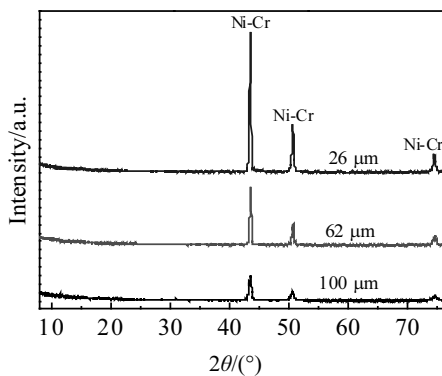


Fig.7 XRD patterns of Ni-based superalloy powders with different particle sizes

surface area, M is the number of nucleants per area. If the diameter of the powder is d , then the surface area of the powder is

$$a = \pi d^2 \tag{2}$$

thus we can obtain:

$$X = \exp[-M\pi d^2] \tag{3}$$

where we assume the $M=10^8$ nucleant/m² [14,15]. Based on Eq.(3) as well as the data available in Table 2, the relation between X and d can be illustrated in Fig. 8. It showing that approximately 4.32% of the powders nucleates at a temperature lower than the equilibrium solidification temperature of 100 μm powders, which means that about 95.68% of these powders nucleate at equilibrium solidification temperature, and only 4.32% of the powders contribute to enhancing the undercooling. In contrast, for 58 μm powders, the corresponding fraction reaches 34.76% and 65.24%, respectively, which means that 34.76% of the powders help to enhance the undercooling; to 20 μm powders, the ratio even reaches 99.98% and 0.02% respectively, which means that 99.98% of the powders nucleate at a temperature lower than the equilibrium solidification temperature, and 99.98% of the powders contributes to enhancing the undercooling [16]. So, the smaller the powder size, the higher the nucleate-free fraction, and the greater the contribution to the undercooling, which is consistent with the test results in Table 2 and Fig.3.

3.2 Effect of cooling rate on the undercooling of powders

Cooling rate is an important factor that can affect undercooling when melt solidifies. But cooling rate is a continuous variable that is not easily measured during the experiment. During the gas atomization, the cooling rate of the

melt droplets can be expressed by the equation^[9,12]:

$$\frac{dT}{dt} = \frac{6h}{d\rho C}(T_d - T_g) \tag{4}$$

where T , T_d , T_g are the droplet temperature, the initial temperature of the melt droplets and the gas temperature, respectively, h is heat transfer coefficient, ρ is melt density, d is the diameter of the powder, C is specific heat of the melt. For different powder sizes, T_d , T_g , ρ , C are constant, so the cooling rate $-dT/dt$ mainly depends on the powder diameter d . From the equation, it is obvious that the smaller the powder size, the faster the cooling rate.

While the relation between the undercooling and the cooling rate can be expressed by the expression^[11, 17]:

$$\ln \frac{\Delta T}{v} = -\ln(s\Omega) + \frac{Af(\theta)\sigma^3 T_m^2}{\Delta H^2 \Delta T^2 kT} \tag{5}$$

where v is cooling rate, ΔT is undercooling, s is the catalytic surface area, Ω is used to present the logarithmic factor, σ is liquid-solid interfacial energy, A is nucleus shape factor, T is solidification temperature, ΔH is melting enthalpy, T_m is equilibrium melting temperature, $f(\theta)$ is the factor of nucleated contact angle, k is Boltzmann constant.

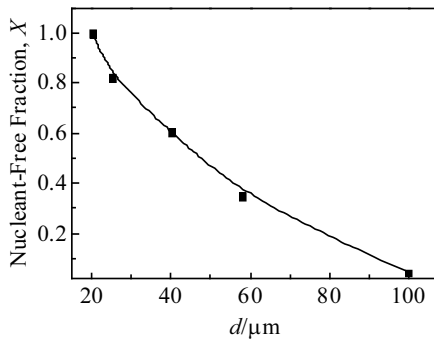


Fig. 8 Relation of the nucleant-free fraction X versus the powder size d

Rearranging Eq. (5), it will be express as:

$$\ln \Delta T = \frac{Af(\theta)\sigma^3 T_m^2}{\Delta H^2 \Delta T^2 kT} = \ln v - \ln s\Omega \tag{6}$$

In Eq.(6), only ΔT and v are variables, and the others are constants, so it is easy to conclude that the undercooling ΔT increases with increasing cooling rate v , which is consistent with the test result of Table 3.

In light of the theoretical analysis and test results achieved above, it is obvious that a high cooling rate will result in a large undercooling.

3.3 Morphology and microstructure of powders

The dependence of mass distribution on the particle size is shown in Fig.2. It is indicated that most of powders are below 48 μm in diameter (>60%). The solidification microstructure of alloy powders has been documented to be closely related to the level of undercooling and cooling rate^[10,18,19]. The powders have good spherical morphology in general, as shown in Fig.5. Besides, there are some particles being capped with small particles. This is because of the inter-collision between melt droplets before their solidification during atomization, which is helpful to improving the powder packing efficiency^[20,21].

There is a lower solidification rate and a smaller undercooling for larger particles due to the slow heat transfer rate, whereas a higher solidification rate and a larger undercooling for smaller particles. With increasing cooling rate and large undercooling, the dendrite arm spacing of particles decreases, and the dendritic crystal will turn into cellular grains^[22-24]. The smaller the particles, the greater the proportion of cellular grain (Fig. 5), and the finer the grain size (Fig. 6).

The microstructure morphology of the cross section of gas atomized Ni-based superalloy powders with different particle sizes is shown in Fig.9. As can be seen in Fig.9, to the internal microstructure of powders, the smaller particle has finer grains. Furthermore, with decreasing particle size, the cooling rate and large undercooling increase, which contributes to an increase in the proportion of cellular grains. So it is consistent with the status of surface, as shown in Fig. 5.

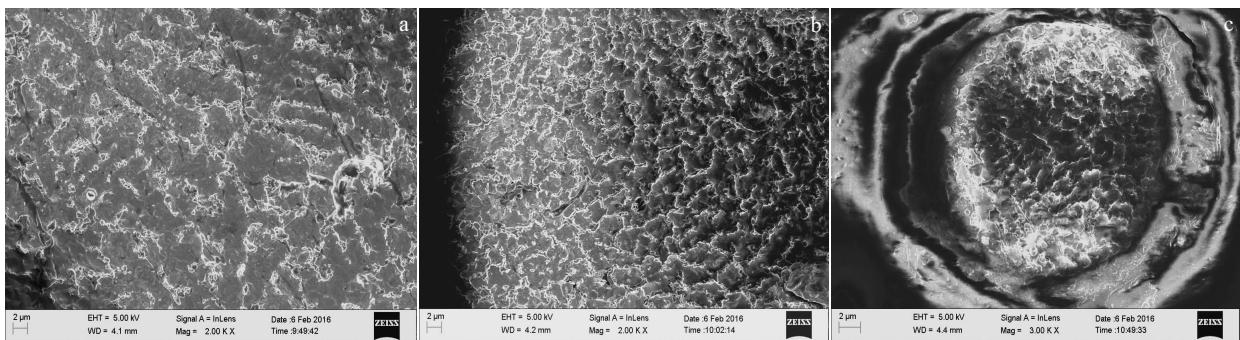


Fig. 9 Microstructures of cross section of gas atomized Ni-based superalloy powders with different particle sizes: (a) 160 μm , (b) 100 μm , and (c) 23 μm

4 Conclusions

1) The Ni-based superalloy powders through gas atomization have good spherical morphology. Keeping the cooling rate constant during atomization, the smaller the powder size, the larger the undercooling and the higher the nucleate-free fraction, and then the greater the contribution to the undercooling.

2) Cooling rate can significantly affect the undercooling of the melt droplets during atomization. In light of the theoretical analysis and test results, it is proved that a high cooling rate will result in a large undercooling.

3) Different undercooling brings remarkable differences in the microstructure of powders. With increasing the cooling rate and large undercooling, the dendrite arm spacing of particles decreases. The smaller the powder size, the larger the proportion of cellular grains, and the finer the grain size of the powder.

References

- 1 Le Guomin, Li Qiang, Dong Xianfeng. *Rare Metal Materials and Engineering*[J], 2017, 46(4): 1162 (in Chinese)
- 2 Achelis L, Uhlenwinkel V. *Materials Science and Engineering A*[J], 2008, 477: 15
- 3 Xie Lichuan, Peng Chaoqun, Wang Richu. *Rare Metal Materials and Engineering*[J], 2015, 44(4): 1006 (in Chinese)
- 4 Cai Zhiyong, Wang Richu, Peng Chaoqun. *Rare Metal Materials and Engineering*[J], 2016, 45(4): 1018 (in Chinese)
- 5 Schwenck Daniel, Ellendt Nils, Fischer-Buehner et al. *Powder Metallurgy*[J], 2017, 60(3): 198
- 6 Lagutkin S, Achelis L, Sheikhaliev S et al. *Materials Science and Engineering A*[J], 2004, 383(1): 1
- 7 Fuqian Z, Ming X, Jianliang L et al. *Materials Science and Engineering A*[J], 2001, 304(1): 579
- 8 Bergmann D, Fritsching U, Bauckhage K. *International Journal of Thermal Sciences*[J], 2000, 39(1): 53
- 9 Mueller B A, Perepezko J H. *Journal of Alloys and Compounds* [J], 1987, 18(1): 1143
- 10 Perepezko J H, Sebright J L, Höckel P G et al. *Materials Science and Engineering A*[J], 2002, 326(1): 144
- 11 Guan W B, Gao Y L, Zhai Q J et al. *Materials Letters*[J], 2005, 59 (1): 1701
- 12 Gao Y L, Guan W B, Zhai Q J et al. *Science China Series E: Technology Science*[J], 2005, 48(1): 632
- 13 Guan W B, Gao Y L, Zhai Q J et al. *Chinese Science Bulletin*[J], 2005, 50(1): 929
- 14 Guan W, Gao Y, Zhai Q et al. *Journal of Materials Science*[J], 2004, 39: 4633
- 15 Jiang H, Moon K S, Dong H et al. *Physics Letters*[J], 2006, 429: 492
- 16 Yang B, Gao Y, Zou C et al. *Chinese Science Bulletin*[J], 2010, 55: 2063
- 17 Zhai Q J, Gao Y L, Guan W B. *Materials Science and Engineering A*[J], 2006, 441: 278
- 18 Dong P, Hou W L, Chang X C et al. *Journal of Alloys and Compounds*[J], 2007, 436: 118
- 19 Park W W, You B S, Kim N J. *Materials & Design*[J], 1996, 17: 255
- 20 Cai Z, Zhang C, Wang R et al. *Materials & Design*[J], 2015, 87: 996
- 21 Dunkley J. *Metal Powder Report*[J], 2002, 57: 18
- 22 Kondoh K, Hamada E L S A, Imai H et al. *Materials & Design* [J], 2010, 31: 1540
- 23 Metz R, Machado C, Houabes M et al. *Journal of Materials Processing Technology*[J], 2007, 189: 132
- 24 Cheng Z, Lei C, Huang H et al. *Materials & Design*[J], 2016, 97: 324

气雾化镍基高温合金粉体的过冷度和显微组织特征

陈仕奇¹, 逯峙², 王广欣²

(1. 中南大学 粉末冶金国家重点实验室, 湖南 长沙 410083)

(2. 河南科技大学 高纯材料研究中心, 河南 洛阳 471023)

摘要: 雾化技术是一种获得微细球形合金粉体的有效方法, 其中雾化过程中的过冷度是影响粉体性能的重要因素。借助 DSC 等实验手段, 研究了镍基高温合金粉体尺寸和冷却速度对粉体过冷度和显微组织的影响, 以及粉体尺寸, 冷却速度和过冷度之间的关系。结果表明, 粉体尺寸和冷却速度越小, 粉体冷却时的过冷度越大。同时, 较大的过冷度会显著降低粉体中树枝晶的臂间距。另外, 粉体尺寸越小, 粉体中的胞状晶的比例越高, 晶粒的尺寸也显著减小。

关键词: 雾化; 粉体; 过冷度; 镍基合金

作者简介: 陈仕奇, 男, 1967年生, 硕士, 副教授, 中南大学粉末冶金国家重点实验室, 湖南 长沙 410083, E-mail: chenpm450@163.com